Fluid flow and mixing in rough-walled fracture intersections

Joel Johnson,[1] Stephen Brown,[1] and Harlan Stockman[2]

Received 5 October 2005; revised 14 August 2006; accepted 31 August 2006; published 23 December 2006.

[1] Fracture intersections play a basic role in contaminant transport through fracture networks because they allow different fluids to mix and disperse along the flow paths. We use experimental and numerical methods to understand and improve predictions of these phenomena. Laboratory experiments of mixing between two miscible fluids were performed within an artificial, rough-walled fracture intersection made of textured glass. We also develop a numerical model of mixing based on local application of streamline routing within the irregular aperture distribution of the intersection. This model shows good agreement with the laboratory experiments, both in the amount of average mixing and in the spatial distribution of dye streamlines. The numerical model is used to generalize our results based on aperture statistics, and shows that mixing is significantly affected by how well apertures correlate across the intersection, especially as fractures are closed. We conclude that flow channelization through rough-walled intersecting fractures significantly enhances physical mixing compared to intersecting parallel plates. Relative to transport through parallel plate aperture networks, surface roughness may reduce solute dilution and increase solute dispersion.

Citation: Johnson, J., S. Brown, and H. Stockman (2006), Fluid flow and mixing in rough-walled fracture intersections, *J. Geophys. Res.*, *111*, B12206, doi:10.1029/2005JB004087.

1. Introduction

[2] Surface and subsurface rocks are pervasively fractured, providing discrete paths for groundwater flow. Fracture networks often have a great deal of heterogeneity in fracture lengths, orientations and apertures, making it difficult to accurately predict flow and especially solute transport [*Berkowitz and Scher*, 1998]. Better predictions of the breakthrough times, spatial distributions and concentrations of solutes in fracture networks based on limited data continue to be critical for effective contaminant remediation.

[3] A universal feature of flow through rough-walled fractures is fluid channeling, in which interconnected pathways of larger apertures transport a significant fraction of the total flow. Channeling in single fractures has been observed experimentally [e.g., *Pyrak-Nolte et al.*, 1987; *Brown et al.*, 1998] and in field studies [e.g., *Bourke* 1987] and is characterized by a wide distribution of flow velocities spread among the different channels [*Brown et al.*, 1998]. Channeling causes increasing deviation from parallel-plate behavior as the fracture walls are closed [e.g., *Brown*, 1987; *Brown et al.*, 1998; *Thompson and Brown*, 1991; *Nicholl and Detwiler*, 2001].

[4] Channeling of fluid flow naturally leads to spatial heterogeneity in fluid compositions. As two different fluids meet and mix at fracture intersections, there is potential for chemical interaction and enhanced fluid-rock interaction. Depending on the fluid compositions, mixing can induce either dissolution of the fracture wall rock or precipitation of minerals in the fractures. Such behavior can have marked implications for understanding and exploitation of geothermal systems, understanding the formation of ore deposits including the statistics of the spatial distribution of ores, in situ leaching for solution mining, and prediction of behavior of groundwater interaction with heat-producing waste canisters.

[5] Despite the knowledge that fracture surface roughness imparts channeling in individual fractures, parallel-plate apertures have been assumed for most research on solute mixing within individual fracture intersections [e.g., *Hull and Koslow*, 1986; *Robinson and Gale*, 1990; *Berkowitz et al.*, 1994; *Li*, 1995; *Stockman et al.*, 1997; *Park and Lee*, 1999; *Li*, 2002]. These studies provide two useful end-member cases to consider: streamline routing and complete mixing [*Hull and Koslow*, 1986]. Streamline routing occurs when two fluids meet in the intersection and based on their relative flow rates are partitioned into the outlet legs along established streamlines in the flow, with most flow routed into the adjacent rather than opposite fracture (Figure 1). In this model, the separate fluids do not mix across streamlines (i.e., molecular diffusion is negligible compared to fluid advection). For streamline routing in parallel-plate intersections, the outlet concentrations depend only on the ratio of inlet to outlet flow rates for adjacent legs of the intersection. In two dimensions, one outlet will always contain pure inlet solution and the other will contain either a pure fluid or an inhomogeneous mixture of the two fluids (Figure 1).

[6] In contrast, complete mixing occurs when the two fluids enter an intersection and are completely mixed so that the fluids exiting through each outlet fracture of the intersection are homogeneous and identical in composition. If

[1]New England Research, White River Junction, Vermont, USA.
[2]Sandia National Laboratories, Albuquerque, New Mexico, USA.

0148-0227/06/2005JB004087$09.00

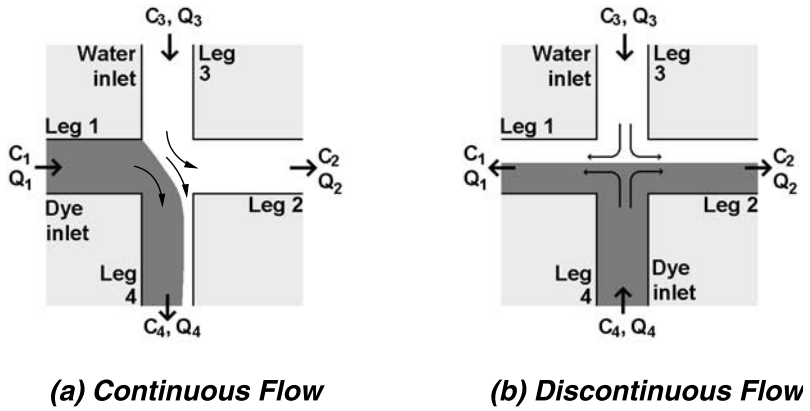

Figure 1. Two-dimensional parallel-plate fracture intersection mixing models. (a) Schematic of continuous flow showing streamline routing with $Q_4 > Q_2$. Leg 4 shows "forced mixing" with inhomogeneous outlet fluid. C is fluid concentration, and Q is flow rate. (b) Discontinuous intersection flow with streamline routing.

flow through the fractures is slow enough, molecular diffusion in the intersection will homogenize the inlet fluids [e.g., *Berkowitz et al.*, 1994; *Li*, 1995; *Stockman et al.*, 1997]. *Park and Lee* [1999] derived analytical solutions to intersection mixing that include both advection and diffusion. Complete mixing maximizes solute dilution and dispersion, while streamline routing represents minimum dilution and mixing through parallel plate intersections.

[7] Numerical and experimental studies of contaminant dispersion through large fracture networks have also generally assumed parallel-plate apertures and two-dimensional flow [e.g., *Robinson and Gale*, 1990; *Berkowitz and Scher*, 1998; *Park et al.*, 2001]. In a network of multiple intersecting parallel-plate fractures, *Hull et al.* [1987] found experimentally that streamline routing rules alone could not fit the solute dispersion they observed. When the models were modified to allow diffusion along the fractures and streamline routing in the intersections the fit to experimental data improved. Similarly, *Bruderer and Bernabe* [2001] modeled flow and solute dispersion through a two-dimensional network of square capillary tubes, each with its own hydraulic transmissivity. Both diffusion and advection were included for solute transport through individual capillaries, but diffusion was ignored in intersections. Streamline routing (i.e., advection alone) was applied at the intersections to calculate solute redistribution along flow paths.

[8] *Park et al.* [2001] conducted simulations of flow and solute transport through a two-dimensional (2-D) parallel plate network with variable aperture distributions. The analytical mixing rules of *Park and Lee* [1999] were used to account for both advective and diffusive processes. They found that the wide distribution of high and low intersection flow rates meant that many intersections were either at complete mixing (diffusion $\gg$ advection) or streamline routing (advection $\gg$ diffusion) conditions. They concluded that streamline routing was a more accurate end-member model than complete mixing, and suggested that streamline routing alone may provide a good approximation to solute dispersion in many cases. In a subsequent study, *Park et al.* [2003] included the complicating factor of three dimensionality in realizations of parallel plate fracture networks, and found that flow in and around intersecting fractures oblique to the dominant pressure gradients led to flow circulation patterns that could significantly retard the transport time of low-concentration solute tails.

[9] Looking at individual intersecting fractures, *Kosakowski and Berkowitz* [1999] acknowledged that orthogonal parallel plates are a poor representation of natural fracture intersections and simulated inertial flow effects through more realistic intersection geometries, although still only in two dimensions and assuming parallel-plate apertures away from the intersection. More recently, surface roughness has been explicitly considered for mixing within intersections. *Stockman et al.* [2001] and *Mourzenko et al.* [2002] numerically simulated surface roughness effects on mixing through both variable aperture and parallel-plate intersecting fractures. Flow regimes where both advection and diffusion processes are important were considered. In those simulations, mixing increased in rough-walled fractures compared to parallel-plate apertures, even when molecular diffusion was negligible. Similarly, we [*Johnson and Brown*, 2001] directly visualized flow and mixing in transparent epoxy replicas of natural rock fracture intersections under flow conditions with negligible diffusion. We observed significant increases in average mixing through the rough-walled fractures over parallel plate streamline routing predictions. We suggested that the deviations from parallel-plate mixing were primarily caused by flow channelization, which results in a wide distribution of flow rates entering and exiting the intersection. However, in these natural samples the rock fracture intersection geometries were too complicated to measure accurately in three dimensions, making it difficult to further evaluate mixing hypotheses.

[10] Here we expand on the previous work by conducting further laboratory experiments in a less complicated synthetic sample. We present a simple numerical model that accurately reproduces the new experimental results. We describe how a new artificial fracture intersection was constructed using textured glass sheets as a fracture analogue with variable apertures. Following *Johnson and Brown* [2001], we conduct laboratory experiments on the mixing of two miscible fluids within the analogue fracture

intersection and also accurately measured fracture apertures. Next, we use the Reynolds equation to numerically simulate laminar flow through the experimentally measured aperture fields. We predict solute mixing in the intersection by locally applying the parallel plate streamline routing model at each grid point along the intersection. The close correspondence in solute transport observed between the laboratory experiments and numerical simulations supports the interpretation that streamline routing applies locally at the intersection, and that patterns of flow channelization set by rough fracture apertures may dominate intersection mixing.

[11] The paper is organized as follows. First, we present relevant background information on streamline routing and mixing. Next, we describe the experimental design and fracture apertures measurements and introduce the Reynolds equation model (REM) which is used to simulate intersection mixing. We then compare measurements of experimental mixing to the numerical model simulations, and conclude that the model sufficiently captures the observed mixing behavior. We use the validated numerical model to generalize intersection mixing as a function of aperture statistics. We use a fractal model of fracture apertures [*Brown*, 1995] to systematically vary surface separation, aperture correlation across intersections, surface roughness and aperture anisotropy.

2. Background

[12] We limit our consideration to single phase flow through two fractures intersecting at right angles. Two of the four fracture legs are inlets, and two are outlets. Two geometries of intersection flow are considered, referred to by convention as "continuous" and "discontinuous" [*Hull and Koslow*, 1986; *Berkowitz et al.*, 1994]. Continuous flow through an intersection occurs when both inlet legs are adjacent to one another (Figure 1a). This case is presumed to be most common in nature. Discontinuous flow occurs when fluid comes in through opposite and parallel legs of one fracture, and exits through the other two parallel legs (Figure 1b).

[13] Mixing of two fluids in an intersection is described by considering the geometry of flow. Here we assume two orthogonal intersecting parallel-plate fractures, effectively in two dimensions. This end-member case is denoted as parallel-plate streamline routing. For continuous flow under these conditions, mixing depends only on the volume flow rates into and out of the intersection and on the inlet concentrations [*Hull and Koslow*, 1986]: If $Q_1 < Q_4$, then

$$C_4 = C_1\left(\frac{Q_1}{Q_4}\right) + C_3\left(1 - \frac{Q_1}{Q_4}\right),$$
$$C_2 = C_3.$$

and if $Q_1 \geq Q_4$, then

$$C_4 = C_1,$$
$$C_2 = C_3\left(\frac{Q_3}{Q_2}\right) + C_1\left(1 - \frac{Q_3}{Q_2}\right). \quad (1)$$

Here C is concentration, Q is volume flow rate, and subscripts reference the individual fracture legs meeting at the intersection shown in Figure 1a. *Robinson and Gale* [1990] suggest the term "forced mixing" to describe the case where one outlet leg has inhomogeneous fluid from both inlets, as always occurs for parallel plate streamline routing.

[14] Discontinuous flow occurs when fluid comes in through opposite (parallel) legs of one fracture, and exits through the other two parallel legs (Figure 1b). For discontinuous flow, streamline routing predicts that both outlet fluids will have the same average concentration [*Hull and Koslow*, 1986]:

$$C_1 = C_2 = \frac{C_3Q_3 + C_4Q_4}{Q_3 + Q_4}. \quad (2)$$

[15] In contrast, complete mixing occurs when both outlet fluids are a homogeneous mixture of the two inlet fluids. A mechanism for complete mixing is molecular diffusion, which will tend to homogenize the fluid concentrations at very low flow rates [*Li*, 1995]. The Peclet number is used to quantify the relative importance of advective to diffusive processes. It is defined as the dimensionless ratio $P_e = ur/D_m$, where D_m is the solute diffusion coefficient, u is the average fluid velocity, and r is a characteristic length scale, in this case of the pore or fracture geometry [*Berkowitz et al.*, 1994]. By convention from previous orthogonal parallel-plate studies, r is defined as half of the diagonal length across the intersection [e.g., *Berkowitz et al.*, 1994; *Stockman et al.*, 1997; *Park and Lee*, 1999]:

$$r = \sqrt{\left(w_1^2 + w_2^2\right)}/2, \quad (3)$$

where w_1 and w_2 are mean apertures (widths) for each fracture.

[16] For a parallel-plate intersection, at high Peclet numbers streamline routing is the appropriate model, while at low Peclet numbers diffusion dominates and complete mixing applies. At intermediate Peclet numbers, both advection and diffusion are important and the degree of mixing lies somewhere in between the two end-members [*Berkowitz et al.*, 1994; *Li*, 1995; *Stockman et al.*, 1997; *Park and Lee*, 1999; *Mourzenko et al.*, 2002]. For parallel-plate intersections, both streamline routing and complete mixing end-member cases have been observed experimentally and predicted numerically [*Berkowitz et al.*, 1994; *Li*, 1995; *Stockman et al.*, 1997; *Park and Lee*, 1999]. *Stockman et al.* [2001] used 3-D lattice Boltzmann numerical methods to study flow and mixing through various fracture intersection representations, highlighting the dependence of mixing on Peclet number. *Stockman et al.* [2001] and *Johnson and Brown* [2001] also showed that when rough-walled apertures lead to flow channelization, advection of fluid as well as molecular diffusion can significantly increase average mixing.

[17] For solute transport through a parallel plate network, streamline routing always directs the maximum possible amount of flow out an adjacent outlet fracture and the minimum out an opposite fracture [*Park et al.*, 2001], giving the least dispersion possible. Essentially we define mixing as deviations from the parallel plate streamline routing model. In this paper, an increase in mixing means

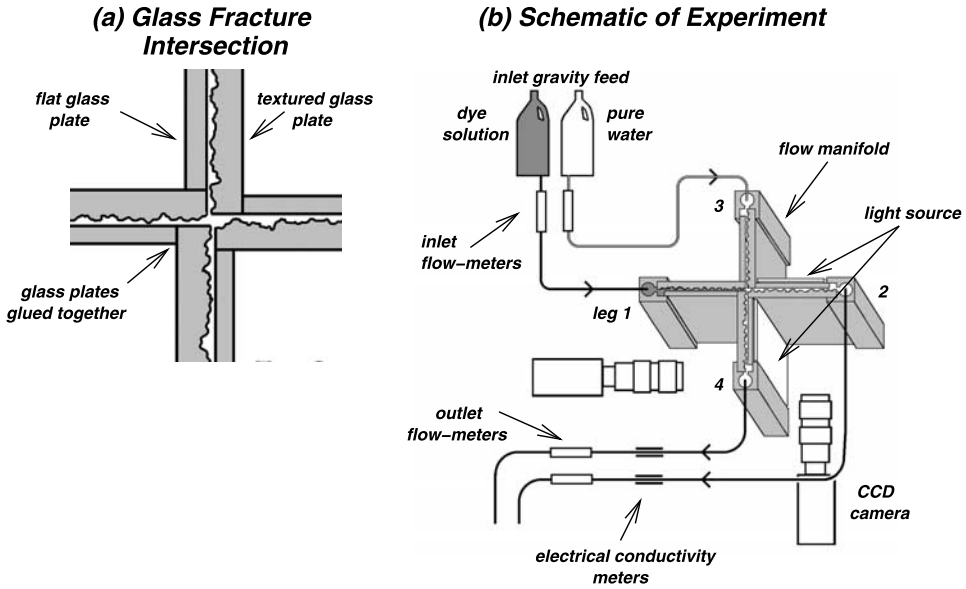

Figure 2. Fracture intersection flow cell. (a) Closeup diagram of the sample intersection as viewed from above, showing how the textured and flat glass sheets were aligned and glued together. (b) Schematic of experimental setup, showing sample inlets and outlets configured for a continuous flow experiment. Sample is viewed obliquely from above. Needle valves used to control flow rates are not pictured. The inlet gravity feed containers were configured to maintain a constant head, giving steady flow rates. Digital cameras provide aperture and dye concentration data at the outlets during the experiments.

that an increased amount of inlet fluid exits through the opposite outlet relative to the adjacent outlet and a decrease in mixing means that more fluid exits through the adjacent outlet. We note that this definition says nothing about the homogenization of solute concentrations within the outlet fluid; it is based on the average concentration of solute in the outlet fractures, rather than on the distribution of solute concentrations.

3. Experimental Design

[18] Using pieces of textured and flat glass we constructed a synthetic "fracture" intersection for laboratory study (Figure 2a). Textured glass has been used previously as a rough-walled fracture analog, since apertures and flow can be directly measured with digital imaging techniques [*Nicholl et al.*, 1999; *Detwiler et al.*, 1999]. Our specimen consisted of four fracture legs, each approximately 6 cm square, meeting at right angles. Flow manifolds on each fracture leg distributed fluid along the edge of each aperture. Apertures for opposite (parallel) legs did not consistently correlate across the orthogonal fracture, because the four textured glass pieces were cut from different places on the glass sheet.

[19] The experimental setup for measuring the aperture fields, the solute concentrations, and fluid flow rates was the same as that of *Johnson and Brown* [2001]. The intersection of the experimental sample was oriented vertically; the mean flow direction through the four sample legs was horizontal (Figure 2b). Two sample legs acted as flow inlets, one for weak dye solution (Rhodamine dye, 1 g/L) and one for distilled water. We used a gravity-fed system with constant head reservoirs of our own design to attain steady flow conditions to the inlet fractures. Flow rates were controlled by adjusting needle valves on each inlet and outlet. We monitored the flow rate of each inlet and outlet with custom flowmeters which consisted of differential pressure transducers used to measure the pressure drop through a length of narrow rigid plastic tubing. The flowmeters were calibrated by measuring flow rates with a stopwatch and scale. Average outlet fluid solute concentrations were determined by measuring the outlet fluid electrical conductivity, because the dye conveniently acted as an electrolyte. Conductivities were measured after the fluid exited the outlet flow manifolds and concentrations were sufficiently homogenized. Flow rates and conductivities were continuously monitored with a data logger and computer. All flow and transport measurements were collected at steady state conditions.

[20] Image analysis gave quantitative measurements of both the aperture distribution and dye concentrations within the sample [*Detwiler et al.*, 1999]. Two CCD cameras (256 gray levels, 640 $\times$ 480 pixels) provided digital images of flow in the fracture during the experiment. The dye was red (Rhodamine wt) and the light source (electroluminescent sheet) was dominantly green, which enhanced the contrast of the dye to pure water. Infrared-reducing camera filters were used to minimize infrared light entering the cameras. We generally followed procedures presented by *Detwiler et al.* [1999] for using images to make quantitative measurements of apertures and dye concentrations.

[21] The Lambert-Beer law relates monochromatic dye absorbency to the concentration and aperture at each point in an image:

$$A = \mu C d = \ln \frac{I_{\mathrm{H_2O}}}{I_{\mathrm{dye}}}. \tag{4}$$

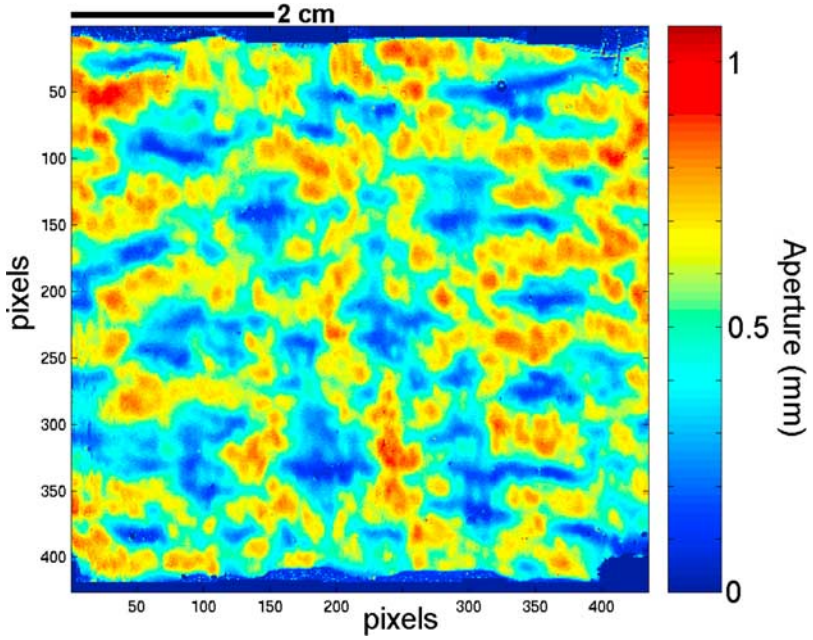

Figure 3. Aperture field for leg 4 of the textured glass measured by dye absorbency as described in the text. The glass we used had anisotropic roughness. Ridges oriented parallel to the flow direction (horizontal in the figure) tended to be more widely spaced than ridges perpendicular to flow (vertical in the figure).

Here A is absorbency, I_{H_2O} and I_{dye} are the measured pixel intensity (gray level) of the apertures filled with pure water or dye solution, μ is the extinction coefficient of the dye, C is dye concentration, and d is aperture. The dye extinction coefficient was measured in a wedge-shaped glass sample with a known linear variation in aperture. The aperture field was then determined by filling the fracture with multiple known dye concentrations, allowing us to correct for nonlinear dye absorbency due to polychromatic light. The measurements at multiple dye concentrations constrains the following empirical curve for the absorbency A:

$$A = \frac{\alpha C}{\beta + C}, \tag{5}$$

with α and β as fitting parameters. Because the importance of the polychromatic component of absorbency decreases as concentration C decreases, the ratio α/β gives a "linear" absorbency as C goes to zero. Finally, aperture d is calculated at each pixel location using

$$\mu d = \frac{\alpha}{\beta}. \tag{6}$$

[22] After aperture d and the calibration factors α and β are known at each pixel location, the same procedure can be reversed in subsequent experiments to measure unknown dye concentrations at each pixel [*Detwiler et al.*, 1999].

[23] Apertures were measured right up to the intersection for each of the four textured glass pieces before assembling the sample. The measurements completely defined the aperture distribution in space because one surface was flat [*Nicholl et al.*, 1999]. Figure 3 shows an aperture field measured for one of the four legs. Once the sample was assembled, direct view of the intersection was obscured by the orthogonally attached piece of glass, so outlet images of dye concentration from the flow experiments stop several millimeters before the intersection.

[24] Figure 4a shows a histogram of the aperture field in Figure 3. Even though we used a different kind of textured glass which resulted in considerably larger apertures, the shape of the histogram is very similar to the smooth-rough glass fracture described by *Nicholl et al.* [1999]. Additionally, the glass we used had a modest anisotropy in the roughness. Ridges oriented parallel to the flow direction tended to be more widely spaced than ridges perpendicular to flow. This anisotropy shows up in the semivariogram plot (Figure 4b), where variance measured perpendicular to flow becomes uncorrelated at shorter separations than variance measured parallel to flow. The semivariogram shows that roughness is not significantly correlated at longer wavelengths. Thus, at the sample scale the aperture can be treated as a homogeneous random field. *Stockman et al.* [2001] used subsets of these experimentally measured textured glass aperture fields to conduct lattice Boltzmann simulations of flow and intersection mixing. Because of computational limitations their simulations were performed over areas of $\approx 3.8 \times 2.6$ cm, rather than over the whole aperture field ($\approx 12 \times 6$ cm). However, Figure 4b shows that this subset of area is large enough to be statistically stationary, and their average mixing results match ours as will be shown below.

[25] On the basis of the typical experimental flow rate of 2 mL/min and the experimentally derived average aperture for the glass sample of d = 0.53 mm, we estimate the

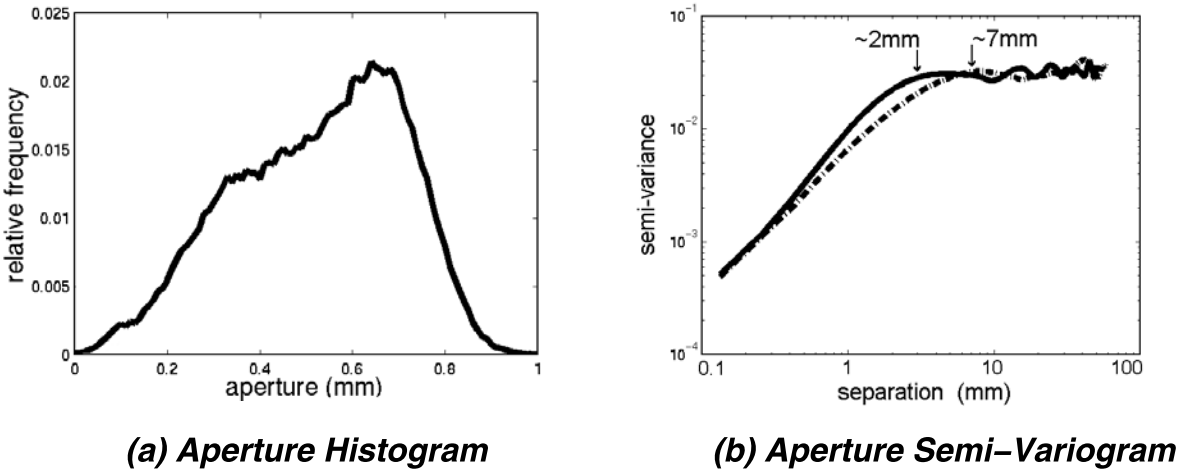

Figure 4. Statistics of the leg 4 aperture shown in Figure 3. The other three glass aperture legs had essentially identical statistics. (a) Aperture histogram indicating a mean aperture of 0.53 mm and standard deviation of 0.18 mm. (b) Semivariograms of the aperture, measured both parallel (dash-dotted line) and perpendicular (solid line) to flow. The roughness anisotropy in the glass shows up in the semivariogram, where apertures measured perpendicular to flow become uncorrelated at a shorter distance (2 mm) than apertures measured parallel to flow (7 mm).

average Reynolds number to be $Re = 0.53$. The Reynolds number, defined here as $Re = ud/v$ with average fluid velocity u, aperture d, and kinematic fluid viscosity v, is the dimensionless ratio of inertial forces to viscous forces. At higher Re, inertia in flow through both individual fractures and fracture intersections can lead to head loss and changes in flow distributions [e.g., *Kosakowski and Berkowitz*, 1999; *Nicholl and Detwiler*, 2001; *Hu et al.*, 2005]. However, numerical simulations of *Kosakowski and Berkowitz* [1999] and *Nicholl et al.* [1999] found that for $Re < 1$ inertial effects are negligible, and are quite small for $Re < 10$. *Stockman et al.* [2001] found similar ranges of insensitivity to Re, and interestingly found that increasing Re decreased mixing ratios in parallel plate fractures, but increased mixing in rough-walled fractures. Even in higher flow rate channels where Re was larger than the mean value, we expect that flow was laminar and inertial effects were likely to be negligible.

[26] The dye solutions were dilute in water and the difference in fluid densities was negligible, so we can express flow rates equivalently by volume/time (appropriate for describing pure water) or mass/time (appropriate for describing the portion of fluid in a mixture originating from the "pure" dye inlet). The density contrast was small enough between the dye solution and pure water that we never observed any flow or overturning associated with density contrasts. Consideration of the Peclet number suggests that mixing from molecular diffusion was also negligible. Estimating a solute diffusion coefficient of $D_m = 7 \times 10^{-6}$ cm^2/s (determined by an empirical method for organic molecules that takes into account molecular weight and chemistry [*Lyman et al.*, 1990], a method with a maximum error of ~10%) and using the average experimental flow rate of 2 mL/min, we estimate the Peclet number to be $Pe = 610$. Various metrics on when the Peclet number indicates significant diffusion have been established in the literature. *Li* [1995], *Stockman et al.* [1997], and *Park and Lee* [1999] found that diffusional mixing is small (~3%) at Peclet numbers >200. *Stockman et al.* [2001] note that for rough-walled intersections the dependence of mixing on Peclet number becomes very small for $Pe \geq 50$. Furthermore, *Berkowitz et al.* [1994] found that streamline routing models provide a good description of mass transfer processes for $Pe > 1$. For our experiments, the mean Peclet number of 610 is high enough to ignore molecular diffusion as a significant mixing mechanism, and our visual observations on the purity of streamlines support this interpretation. Areas of the fractures with flow much slower than the mean velocity (and hence lower Peclet numbers) could have minor diffusional mixing, but stagnating fluid pockets also transport little fluid through the sample. As will be shown, advection clearly dominates dye transport and mixing through our sample.

4. Reynolds Equation Model (REM)

[27] Knowing the detailed aperture field of each experimental fracture leg allows us to simulate fluid flow and mixing through the intersection and to directly compare the numerical and experimental results. To do this, we simultaneously solve the Reynolds equation for flow through both fractures and couple the solutions to account for fluid exchange from one fracture to another through the intersection.

[28] The Reynolds equation describes two-dimensional flow between rough surfaces with smoothly varying aperture. The Reynolds equation assumes that the "cubic law", in which local hydraulic conductivity is proportional to the cube of local aperture, holds locally in the variable-aperture fracture. Considerable deviations can occur between the actual flow field and that predicted by the Reynolds equation when roughness is high relative to the average

aperture [*Brown et al.*, 1995; *Oron and Berkowitz*, 1998; *Nicholl et al.*, 1999; *Detwiler et al.*, 2000; *Nicholl and Detwiler*, 2001]. Despite this fact, the Reynolds equation has been widely used to model flow in rough-walled fractures [*Brown*, 1987; *Thompson and Brown*, 1991; *Nicholl et al.*, 1999; *Detwiler et al.*, 2000].

[29] To model flow in intersecting fractures, we solved the Reynolds equation simultaneously in two separate aperture fields. We solved a finite difference form of the equation by using the iterative method of successive overrelaxation [*Thompson and Brown*, 1991]. The aperture fields were assumed to intersect along a single column of pixels at the center of each fracture. Flow source and sink terms were used at each grid point along this column to simulate an intersection. The fluid pressure at each intersection grid point was forced to be equal in both fractures in during iterative solution of the governing equations, causing flow to be conserved around and through the intersection. Similarly, apertures along the intersecting grid points were set to be equal in both fractures; we chose to set the aperture of each leg equal to the local maximum value of the two initially intersecting apertures. Using the diagonal length across the intersection would only result in most cases in slight and at most a modest factor of $\sqrt{2}$ increase in local intersection aperture. For these simulations in which the average flow direction is perpendicular to the intersection, our results depend on the patterns of flow channelization. This flow channelization depends more on the aperture fields both upstream and downstream (high-aperture interconnectivity allows high-flow channels) and less on apertures right at the intersection. The REM simulations are too simple to include variables such as the average angle between the intersecting fractures, or any kind of explicit flow patterns in the intersection such as described by *Kosakowski and Berkowitz* [1999].

[30] Once the flow field was determined by solving the Reynolds equation, each intersection pixel had two flow rate vectors entering and two exiting (one for each inlet and outlet leg). The discrete nature of the finite difference simulations resulted in small (<2%) mass balance differences at the intersection pixel scale. To compensate, intersection inlet and outlet flow rates were normalized so that flow was exactly conserved at each intersection grid point. To model steady state solute transport and mixing, we assume that parallel-plate streamline routing holds locally at the intersection. Streamline routing (equation (1) or (2)) was applied at each intersection pixel using local flow rates to determine solute concentrations flowing into each outlet leg. Diffusion was not included, so simulations correspond to the high Peclet number limit of streamline routing behavior.

[31] Numerical simulations were designed to match the experimental conditions of the laboratory measurements. Simulations were run using the full aperture fields determined by image analysis for the laboratory sample. Each of the two intersecting fractures modeled by the REM consist of two of the four textured glass apertures and are approximately 420 grid points (pixels) high by 850 long. In the simulations, the average flow rate in each fracture leg was controlled by iteratively adjusting the applied boundary pressure gradient across each fracture so that the mean experimental and numerical flow rates match through each aperture.

5. Results

[32] We present results from laboratory mixing experiments using both the continuous and discontinuous intersection flow conditions and then compare these data to REM predictions. We find a good match between experiments and simulations, thus validating the REM assumptions. A primary result of this study is that rough-walled fractures have more mixing than flow through parallel plates, when diffusion is negligible. Not surprisingly, mixing typically falls between the streamline routing and complete mixing models.

5.1. Continuous Flow Tests

[33] For continuous flow test 1, the inlet flow rates for both dye and water remained constant at 2 g/min each for the entire experiment. The inlet and outlet leg numbers correspond to Figure 1a. The outlet flow rate was varied incrementally in 11 steps, from all flow (4 g/min) coming out leg 1 (leg 4 flow fraction =0), to all flow coming out leg 4 (leg 4 flow fraction =1). Figure 5 shows the mixing results for this test. The same data are plotted in two ways: as dye fraction (Figure 5a), and as dye flux (Figure 5b). Dye fraction gives the average concentration of fluid in each outlet. Dye flux gives the mass flow rate (g/min) of dye solution through the sample. As an example, when the flow fraction in leg 4 is 0.5 (x axis, Figure 5a), outlet fluid adjacent to the pure water inlet (leg 2) contains ~25% dye, while the outlet adjacent to the dye inlet (leg 4) contains ~75% dye. At this flow fraction (reading from Figure 5b), since the dye inlet flow rate is 2 g/min the corresponding dye fluxes through the two outlets are ~0.5 g/min and ~1.5 g/min. The experimental results fall between the parallel plate streamline routing and complete mixing models. In contrast, the REM simulations provide a reasonable match to the homogenized dye concentrations exiting the outlet legs.

[34] Figure 6 shows images of dye concentration in each outlet leg as derived from image analysis for the case of equal inlet and outlet flow rates (flow fraction 0.5). Using the glass specimen aperture fields and the experimental flow parameters, the Reynolds equation model (REM) was used to simulate the dye distribution for this experiment (Figure 6). The concentrations and locations of streamlines in the simulations approximately match those on the experimental images. Simulations also match the experimental flow tortuosity by visual comparison of the irregularity of the dye ribbons.

[35] A similar flow experiment (continuous test 2) was performed with somewhat different flow steps, in which inlet and outlet flows were both varied incrementally from all flow going straight through one fracture to all flow coming through the other fracture (i.e., $Q_1 = Q_2$ and $Q_3 = Q_4$, but Q_1/Q_4 is varied). As the experiment progressed, the inlet flow rate for dye (leg 1) was varied from 4 g/min to zero (flow fraction =0 on legs 3 and 4). At the same time the inlet flow rate for pure water (leg 3) increased from zero to 4 g/min (flow fraction =1 on legs 3 and 4). As before, the numerical simulations match both the average dye fraction

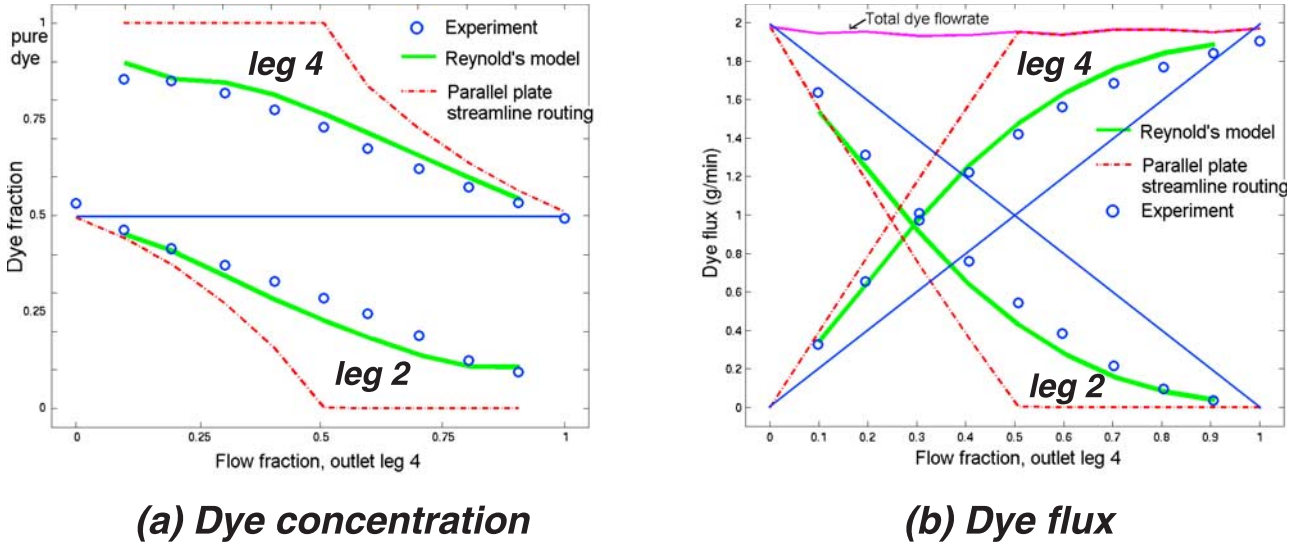

Figure 5. Average mixing through fracture intersection, continuous test 1. Figure 1a shows the configuration of inlet and outlet legs. Inlet flow rates (legs 1 and 3) remained constant and equal during the experiment, while outlet flow rates were varied systematically from all flow exiting through leg 2 to all flow exiting leg 4. The experimental results, the Reynolds equation simulations of flow through the experimentally measured apertures, and the predictions of the 2-D streamline routing mixing model are plotted. (a) Dye fraction (normalized dye concentration) plotted against leg 4 flow fraction (the ratio of flow exiting through outlet leg 4 to the total flow through the sample). The complete mixing model is indicated by the solid blue line. (b) The same data as in Figure 5a, plotted as dye flux through each outlet leg versus flow fraction. Complete mixing model is indicated by the solid blue lines.

and average dye flux (Figure 7) and also match the spatial distribution of dye concentration (Figure 8). Figure 7c shows good agreement among the REM, experiment and lattice Boltzmann (LB) model described by *Stockman et al.* [2001]. The LB simulations are more rigorous characterizations of flow and solute transport through the intersecting fractures than the REM model. They include mixing through molecular diffusion as well as inertial flow effects (although as argued above, the magnitudes of these are small). The REM simulations have much simpler and less realistic models for both flow (local parallel plate flow) and solute transport (local streamline routing), and yet the correspondence between experiments and models demonstrates that they capture the essential physics of intersection mixing at our experimental conditions.

5.2. Discontinuous Flow Tests

[36] Discontinuous flow experiments and simulations were performed using the flow configuration of Figure 1b (see Figure 9). Flow proportioning was similar to continuous test 2, but instead of having equal flow rates in opposite inlet-outlet pairs, flow rates were the same in adjacent inlet-outlet pairs. As the experiment progressed the fraction of dye was varied from 100% to zero. Figure 9 compares mixing from experiments, REM simulations, and the parallel plate mixing models.

[37] For discontinuous flow, both streamline routing and complete mixing models collapse to the same line. Both end-member mixing models predict that the two outlet fluids will have the same average concentration. Complete mixing would have homogeneous outlet fluid, while streamline routing has separate "forced" mixtures of the inlet fluids. Figure 9 shows that the outlet fluids remain close to one another in dye concentration. When flow dominates on one fracture, our experimental deviation from end-member models is consistent with the discontinuous intersection flow patterns calculated by *Philip* [1988] for Laplace and Stokes flow which include changes in flow due to recirculation zones. Our REM simulations predict a small deviation from the end-member models opposite to that observed in our experiments. Since our simulations are too simple to explicitly model flow patterns within the intersection, we do not expect the REM results to match *Philip*'s [1988] results exactly. For this discontinuous case, experimental and numerical images of dye concentration in the outlet legs look similar, although dye streamline concentrations tend to be lower in the simulations.

[38] We summarize our results to this point. First, advection of fluid through rough-walled synthetic fractures considerably enhances mixing compared to parallel-plate streamline routing predictions, even in the absence of molecular diffusion. Outlet concentrations are not uniformly mixed within rough-walled outlet fractures, but consist of ribbons or streamlines of solute. Streamline routing accurately describes mixing in 2-D and between parallel plates, but underestimates mixing when applied to an entire 3-D fracture intersection.

[39] Second, the REM model captures the mixing dynamics observed in the experiments. In these simulations, the fracture intersection was assumed to behave like a large number of stacked individual parallel-plate intersections. This mechanism is sufficient to predict both average mixing and the spatial distribution of solute streamlines. The good match between experiments and simulations further dem-

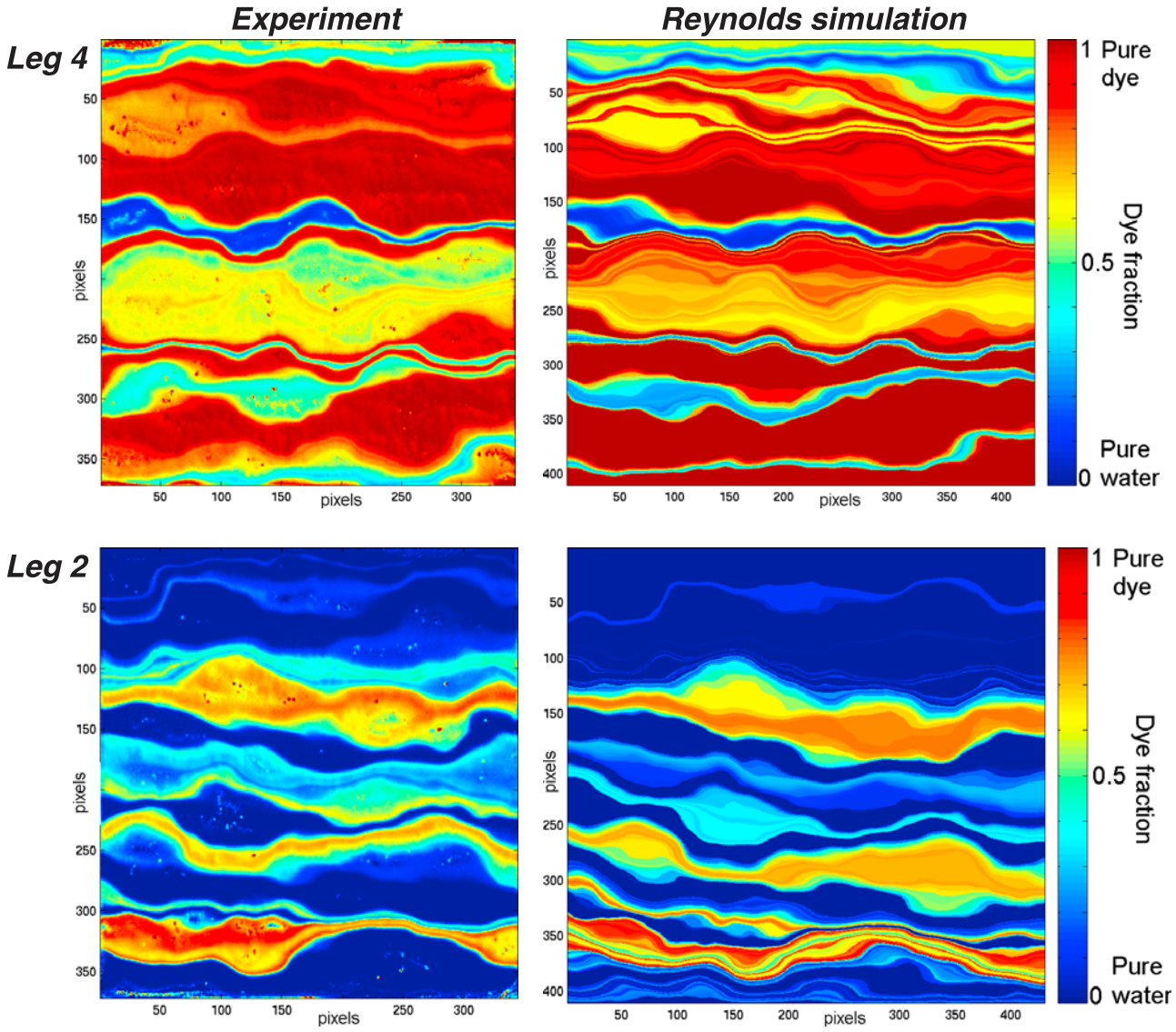

Figure 6. Experimental and simulated outlet concentrations, continuous test 1. Average flow rates are equal for both outlet legs (flow fraction 0.5). The quantitative image analysis methods used to measure experimental dye concentrations are described in the text. Flow is from left to right in each image. The experimental concentration images cover a slightly smaller subset of area than that shown for simulations.

onstrates that patterns of flow channelization in the intersecting fractures dominantly control advection of fluid through the intersection, and hence mixing.

5.3. Parameters Affecting Mixing

[40] Having validated the REM model, we next use it to explore the importance of additional aperture parameters on mixing. *Stockman et al.* [2001] simulated lattice Boltzmann flow through idealized fluted channels and showed that mixing can change dramatically as a function of how well apertures correlate across and around an intersection. Motivated by this finding, we calculate mixing as a function of fracture opening and closing and aperture correlation across the intersection, and also explore surface roughness effects and anisotropy. We conducted simulations in both the textured glass plate aperture fields and in numerical apertures generated with a fractal model for rough-walled fractures [*Brown*, 1995].

[41] Apertures for the REM flow simulations are made by placing two surfaces together at a prescribed normalized surface separation S defined as [*Thompson and Brown*, 1991]

$$S = d_m/\sigma, \tag{7}$$

where d_m is the mean aperture and σ is the standard deviation of the aperture field. Surface separation is changed by adding or subtracting a uniform value from all apertures. The surface separation calculated for the experimental glass apertures when the surfaces are touching is $S \approx 2.9$. Thus, at $S > 2.9$ the surfaces do not touch; at $S < 2.9$ the surfaces touch and material at some locations overlaps at the

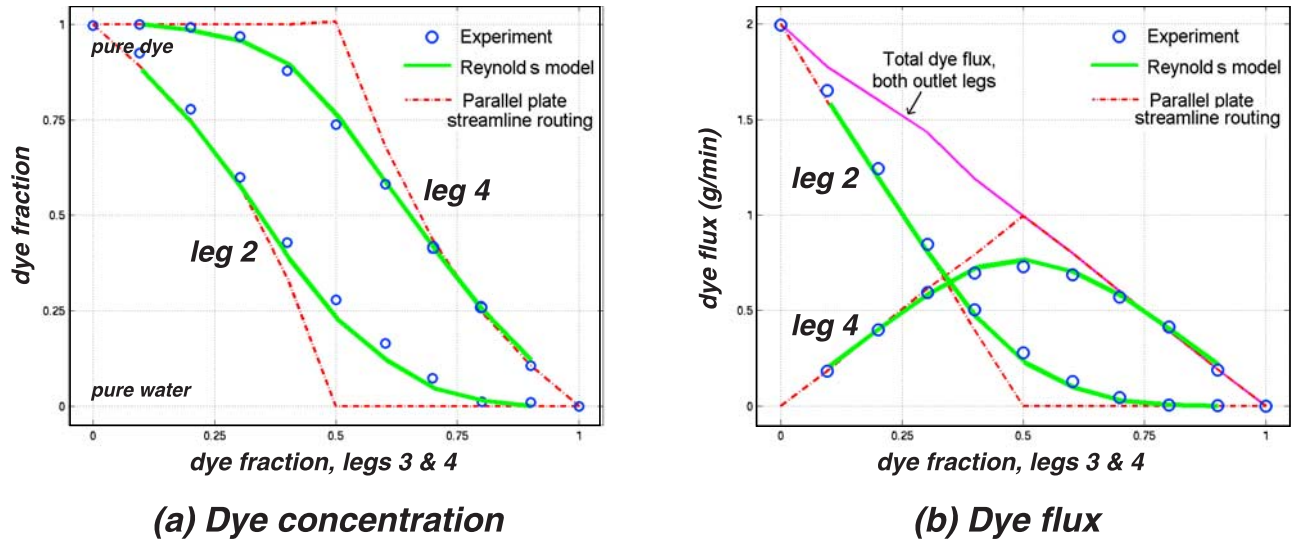

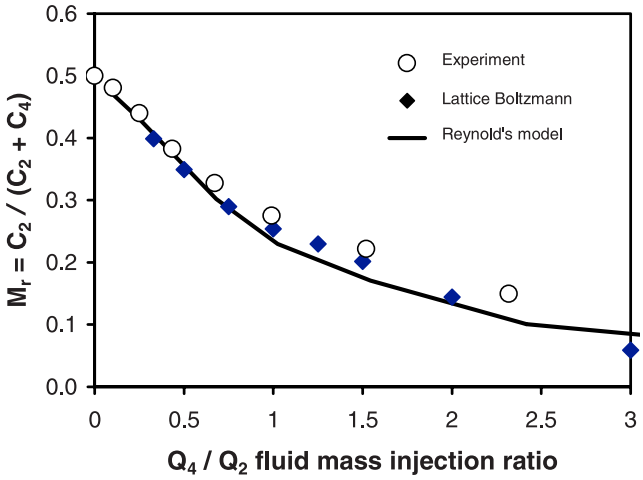

Figure 7. Average mixing through fracture intersection, continuous test 2. Figure 1a shows the configuration of inlet and outlet legs. During this experiment, the total flow rate through the sample remained constant, but inlet and outlet flow rates were varied systematically from all flow through legs 1 and 2 to all flow through legs 3 and 4. (a) Dye fraction versus flow fraction through outlet leg 4 (as well as inlet leg 3). (b) The same data as in Figure 7a, plotted as dye flux through each outlet leg versus flow fraction. (c) Comparison of numerical methods. The same results as Figures 7a and 7b are shown compared to lattice Boltzmann (LB) calculations. The LB code is cast in dimensionless ratios, so for this plot we use the apparent mixing ratio parameter M_r as the basis of comparison.

contacts. In the simulations, the aperture at overlapping contacts was set to zero and the overlapping material was ignored [*Thompson and Brown*, 1991; *Oron and Berkowitz*, 1998].

[42] Because the four textured glass pieces were cut from separate locations, the experimental sample had uncorrelated intersection apertures. To speed the simulations, 300 × 300 pixel subsets were chosen from both of the original textured glass apertures. Simulations were also performed with correlated intersection apertures, constructed by taking two different original glass aperture fields (e.g., Figure 3) and inserting a numerical intersection down the center.

5.3.1. Surface Separation, Uncorrelated Intersection Apertures

[43] Simulations were done for surface separations from 10 to 0.5, using the same flow conditions as continuous test 2 (Figures 7 and 8). Figure 10 shows outlet dye concentrations and dye flux through the sample. The maximum deviation from streamline routing occurs when all inlet and outlet flow rates are equal (flow fraction 0.5), as was

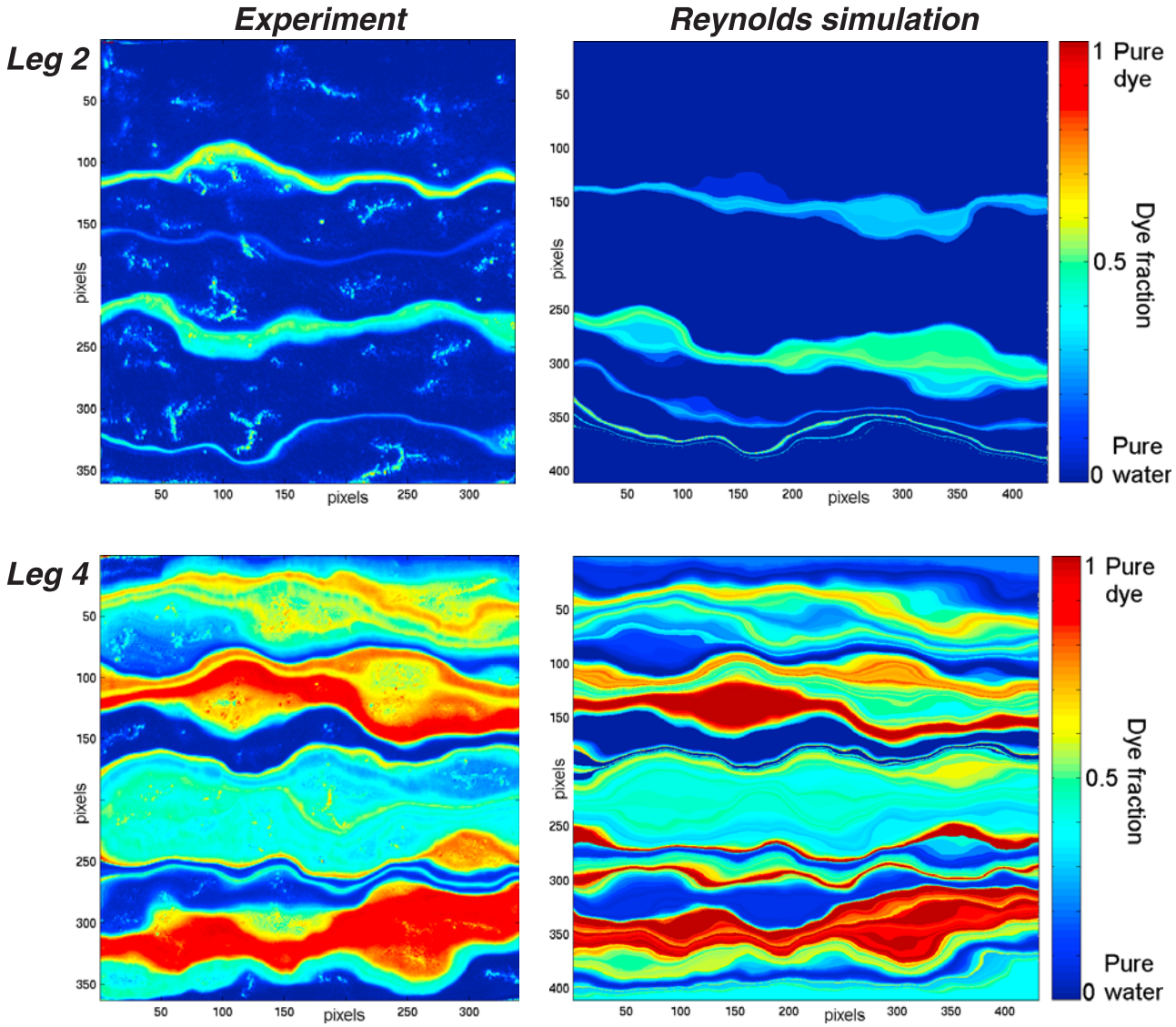

Figure 8. Experimental and simulated outlet concentrations, continuous test 2. Thirty percent of the flow exits leg 2, and 70% exits leg 4 (leg 4 flow fraction 0.7). Flow is from left to right in each image. The experimental concentration images cover a slightly smaller subset of area than that shown for simulations.

generally observed in the previous cases (Figures 5 and 7). Average mixing increases as the fractures are closed. However, at the smallest two surface separations of $S = 1$ and $S = 0.5$ there is little change in mixing with increased closure. Once the fractures closed down beyond a certain point, the few remaining flow channels did not change much in relation to one another and therefore the distribution and concentration of outlet streamlines remained essentially constant.

[44] Parallel-plate streamline routing actually appears to be a good average mixing approximation for much of this experiment: when 30% or less total flow goes through one fracture (flow fraction ≤ 0.3 or ≥ 0.7), dye fluxes are close to streamline routing predictions (Figure 10b). *Park et al.* [2001] describe the case where flow on one fracture dominates total intersection flow as either "apparent streamline routing" or "apparent complete mixing", because simple mass balance means that the models will tend to agree. Near the endpoints, the complete mixing model also comes close to matching the dye fluxes.

5.3.2. Surface Separation, Correlated Intersection Apertures

[45] Simulations were done to study the properties of intersecting fractures with apertures that correlate across the intersection, at surface separations of 6, 3, and 1 (Figure 11). These correlated fractures give higher average mixing than fractures with uncorrelated apertures. For correlated apertures at $S = 3$ the mixing value was 0.32 (Figure 11) compared to 0.22 for uncorrelated apertures (Figure 10). Channels of higher flow correlate across the orthogonal fracture and so more fluid goes straight through the intersection instead of turning to the adjacent outlet. The

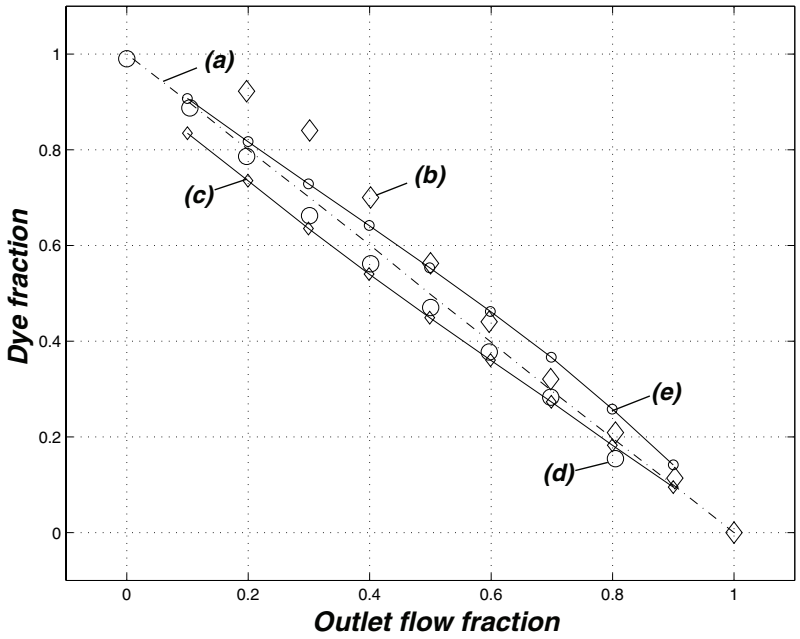

Figure 9. Average experimental and simulated outlet concentrations for the discontinuous test. Figure 1b shows inlet and outlet flow configuration. Complete mixing and streamline routing end-member predictions are identical for discontinuous mixing (dot-dashed line a). Experimental mixing (large symbols) diverges from parallel-plate predictions in the opposite direction to that of the REM simulations (small symbols), yet both do follow the parallel-plate models rather closely. Large diamonds (line b) are experimental dye fractions for outlet leg 2. Large circles (line d) are experimental dye fractions for outlet leg 1. The dot-dashed line a represents both streamline routing and complete mixing parallel plate end-member models. Small diamonds (line c) and small circles (line e) connected by lines are REM simulations for outlet legs 2 and 1, respectively.

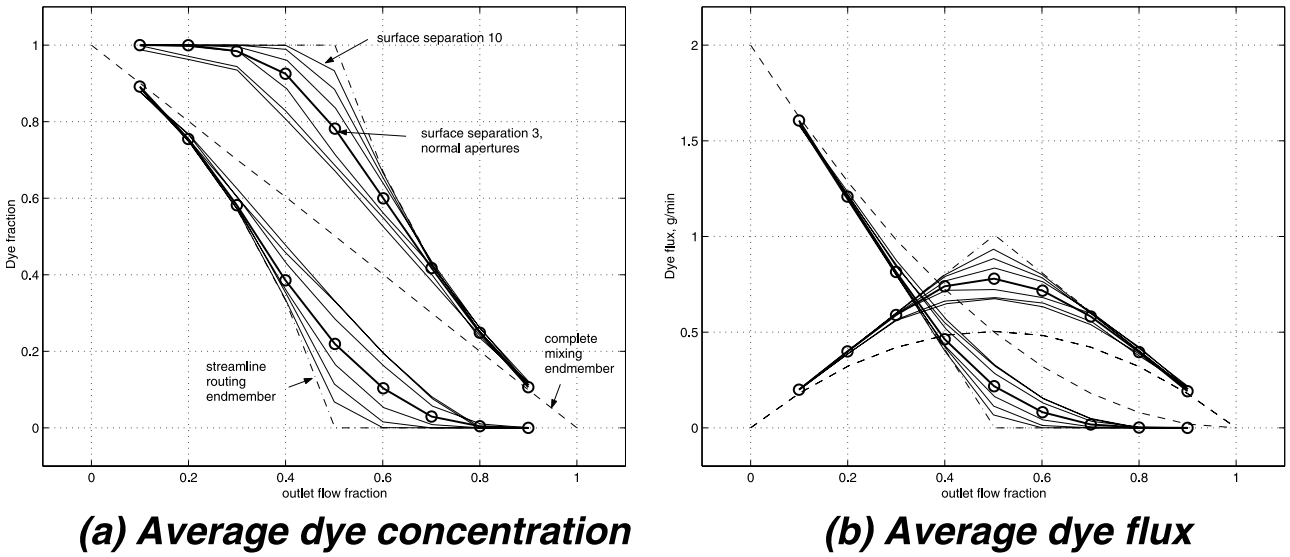

Figure 10. REM flow simulations for mixing through textured glass apertures as the fracture aperture is opened and closed. The fracture apertures do not correlate across the intersection. There are two sets of solid curves representing the surface separations of 10, 6, 4, 3, 2, 1 and 0.5 going from the outside "streamline routing end-member" (dot-dashed line) to the inside "complete mixing end-member" (dashed line). A surface separation of 3 is very close to the experimental surface separation of 2.9. Note that the mixing changes very little for surface separations of 1 and 0.5. (a) Average dye concentration versus outlet flow fraction. (b) Average dye flux versus outlet flow fraction.

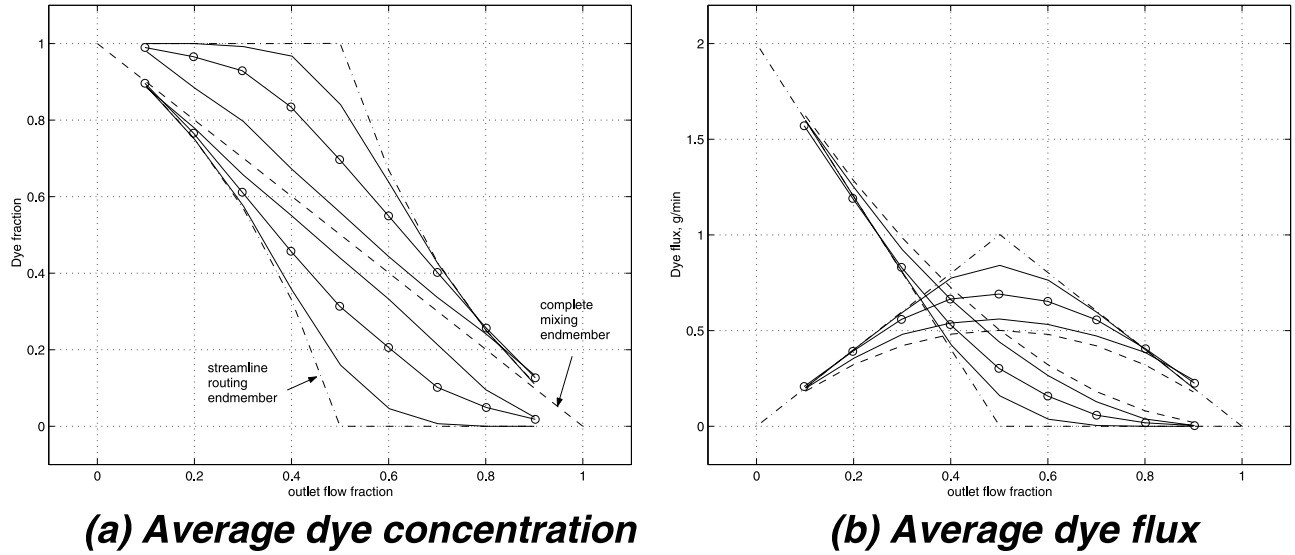

Figure 11. REM flow simulations for mixing through textured glass apertures as the fracture aperture is opened and closed. The fracture apertures are correlated across the intersection. There are two sets of solid curves representing the surface separations of 6, 3, and 1 going from the outside "streamline routing end-member" (dot-dashed line) to the inside "complete mixing end-member" (dashed line). (a) Average dye concentration versus outlet flow fraction. (b) Average dye flux versus outlet flow fraction.

effect of correlated apertures significantly increases as the fracture is closed. With $S = 1$, solute transport through the correlated apertures is reasonably close to complete mixing.

5.3.3. Fractal Surface Roughness and Anisotropy

[46] We explored the additional parameters of surface roughness and anisotropy on mixing, using the fractal fracture model of *Brown* [1995]. Numerically generated fracture surfaces allow aperture parameters to be varied independently in ways difficult or impossible to perform experimentally [*Brown*, 1995, 1987, 1989; *Brown et al.*, 1998; *Thompson and Brown*, 1991]. The mathematical model for simulating fractures allows variations in the fractal dimension, the standard deviation of asperity heights and the mismatch of the two contacting surfaces as determined by a mismatch length scale above which individual fracture surfaces are correlated [*Brown*, 1995]. The fractal dimension describes the scaling of surface roughness. Studies of natural fracture profiles show that the typical range of fractal dimensions is 2 to 2.5, with 2 appearing to the eye as smoother and 2.5 rougher. In addition, the model allows for roughness anisotropy. All of the model variables can be independently varied while keeping the same long-wavelength matching of individual fracture surfaces, giving similar aperture channels for flow. REM mixing simulations were performed in a fractal aperture field with uncorrelated apertures as a function of flow fraction and surface separation. All simulations used equal inlet and outlet flow rates (flow fraction =0.5).

[47] We now briefly summarize the results for fractal surfaces. We found that for smooth isotropic fractal apertures, except for the closest surface separation of $S = 1$, mixing agreed quite well with simulations on the textured glass apertures for both the uncorrelated and correlated cases. We found that varying the fractal dimension (which controls the fine-scale surface roughness) had little effect on average mixing values. Increased fine-scale surface roughness tended to slightly decrease average mixing, meaning that somewhat more fluid flowed around the corner to the adjacent outlet. The effect of this fine-scale roughness increased as the fractures closed, but never changed average mixing by more than approximately 5%. The first-order mixing behavior was still controlled by flow channeling through interconnected larger-aperture areas (long wavelength features), which did not change significantly in these simulations as the fractal dimension was varied.

[48] Anisotropy parallel or perpendicular to the flow had a larger effect on mixing. Longitudinal anisotropy (making the surface roughness look elongated parallel to mean flow) changed mixing very little from the isotropic case, over the range of surface separations studied. However, transverse anisotropy (roughness elongation perpendicular to mean flow) showed interesting behavior. When the fractures were open (higher surface separations), transverse anisotropy retarded mixing, because the anisotropy tended to retard the amplitude of flow channelization. However, at low surface separations as the fractures contacted and closed, transverse anisotropy increased channelization and caused mixing to increase. Long surface contacts perpendicular to the mean pressure gradient forced flow paths to become very tortuous. The few narrow flow channels that remained open transported nearly all of the fluid straight through the intersection, tending to increase mixing.

6. Discussion

[49] This paper explores the advective component of solute transport through intersecting rough-walled fractures. Fundamentally, flow channelization causes the mixing trends and deviations from parallel plate models that we observe. A distribution of flow rates come into and out of

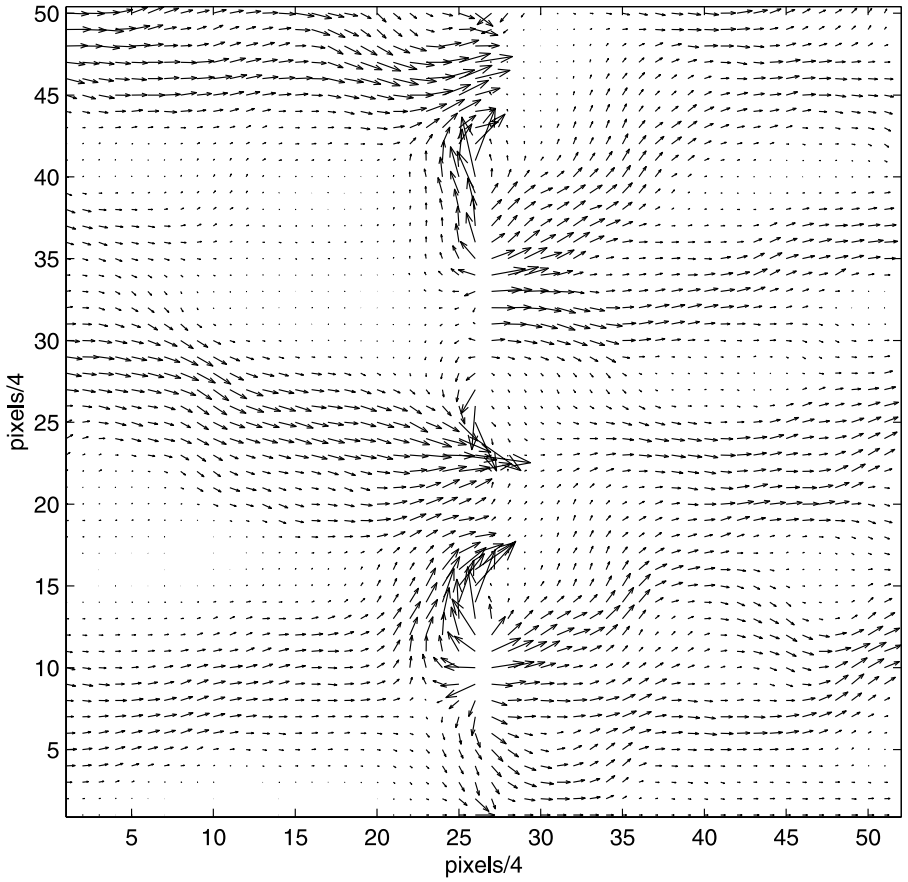

Figure 12. Flow vectors for a subset of an REM flow simulation straddling an intersection. For clarity, only 1/4 of the calculated vectors are shown. The applied pressure gradient drives the average flow from left to right. However, locally at the intersection where flow enters and exits on the other fracture, flow occurs opposite that of the average pressure gradient.

the intersection. As equation (1) predicts when applied locally at the intersection, the distribution of flow rates leads to a distribution of outlet concentrations. Channels distribute fluid from each inlet fracture to both outlet fractures, thus increasing mixing compared to parallel-plate streamline routing predictions. Outlet concentrations are not uniformly mixed within rough-walled intersection outlet legs, but consist of ribbons or streamlines of solute.

[50] The accuracy of the Reynolds equation for modeling 2-D flow has been explored and questioned [e.g., *Brown et al.*, 1995; *Nicholl et al.*, 1999; *Nicholl and Detwiler*, 2001; *Mourzenko et al.*, 2002]. However, the good match between our experiments and REM simulations demonstrates that, for our purposes, the Reynolds equation captures the essential flow channelization that is the first-order control on mixing. This is fortunate since the Reynolds equation is numerically more efficient to solve and easier to implement than more complicated equations such as the full 3-D Stokes equation. Fracture network models could perhaps be developed that directly incorporate fracture surface roughness and flow channelization and therefore could explicitly capture the mixing phenomena we observe.

[51] In simulations of flow through three-dimensional parallel plate fracture networks with complex geometries, *Park et al.* [2003] found that fractures with little net flow will act as local flow paths for intersecting fractures, and that this phenomenon can significantly increase the residence time of solute in the fracture network. Similarly, in the epoxy replicas studied previously we observed that flow from one inlet sometimes locally blocked flow from the other inlet [*Johnson and Brown*, 2001]. We also observed this behavior in the experiments on the glass sample and in the corresponding REM simulations. It is common for local pressure gradients near the intersection to drive flow opposite to the imposed sample-scale pressure gradient (Figure 12). This typically occurs when one outlet leg has relatively little exiting flow; near the intersection it acts as a conduit for flow on the orthogonal leg. The amount of flow blocking in these simulations tends to be small compared to the experiments by *Johnson and Brown* [2001], because of the more idealized geometry of the textured glass apertures. Nonetheless, this ''intersection blocking'' phenomenon can lead to some streamlines maintaining pure dye concentrations in both the opposite and adjacent outlet legs.

[52] Compared to parallel plate apertures, our results suggest that surface roughness may both increase solute dispersion and decrease solute dilution. Both phenomena are particularly significant for contaminant transport. Generally speaking, dispersion refers to the transverse spreading of solute [e.g., *Detwiler et al.*, 2000; *Park et al.*, 2001],

while dilution represents diminished concentrations of solute in a homogeneous mixture [*Kitanidis*, 1994].

[53] Figures 6, 8, and 10 show that dye concentrations follow flow streamlines and remain unchanged in our experiments as flow goes across the outlet legs. The geometry of flow channels may retard diffusional homogenization in both individual fracture legs and intersections by tending to isolate significant volumes of flowing fluid. For slow flow within a parallel plate fracture (depending on the Peclet number), fluid can become homogenized by diffusion before reaching the next intersection [*Hull et al.*, 1987; *Robinson and Gale*, 1990; *Park and Lee*, 1999; *Park et al.*, 2001; *Bruderer and Bernabe*, 2001]. Other processes such as Taylor dispersion or macrodispersion will also tend to homogenize the fluids [*Detwiler et al.*, 2000]. Flow channelization and intersection blocking can locally maintain solute concentrations higher than predicted by parallel plate models. Therefore the advective mixing processes observed here may increase spatial solute dispersion but reduce solute dilution.

[54] Numerical simulations show that mixing approaches parallel-plate streamline routing predictions as fracture apertures are opened because flow channelization decreases. As apertures decrease, flow at the intersection becomes increasingly concentrated within the remaining interconnected open aperture channels. The range of mixing ratios that are expected for natural fracture closure would be between approximately 20% and 40%. Mixing tends to increase with closure, but whether a particular flow channel correlates across (opposite outlet) or around (adjacent outlet) will cause significant variations in mixing from intersection to intersection, even if the fracture aperture statistics are the same. For some samples a limit may be reached beyond which flow channel partitioning around and through the intersection does not significantly change, and increased closure may not affect mixing ratios. Anisotropic roughness modestly affects flow channeling in interesting ways. Longitudinal roughness tends to enhance channeling, slightly increasing mixing. Transverse roughness decreases channeling in open fractures, but tends to increase channeling and mixing in tight fractures.

[55] The differences in mixing observed between these results and those of *Johnson and Brown* [2001] point out that significant differences exist between our idealized glass apertures and real rock fracture intersections. Comparable experiments using epoxy replicas of two natural fracture intersections [*Johnson and Brown*, 2001] gave much higher average mixing values and more variability in mixing than the idealized synthetic glass sample or REM simulations. Collectively, the dependence of mixing on the details of flow channel geometry suggests that significant variability may be inherent in mixing ratios at natural fracture intersections.

7. Conclusions

[56] Solute mixing is significantly enhanced in intersecting rough-walled fractures compared to intersecting parallel plates. Flow through variable aperture fractures leads to flow channelization, and when these fractures intersect the distribution of flow rates means that some flow from each fracture will exit through each outlet fracture, increasing fluid mixing over parallel plate streamline routing.

[57] Because flow channelization is the first-order control on mixing in our rough-walled experimental fracture intersections, a numerical model that uses the Reynolds equation to simulate flow through variable apertures is sufficiently accurate to predict both spatial distributions of dye concentrations within the fractures, and average mixing ratios. The correspondence between experiments and the numerical model demonstrates that advection-dominated streamline routing holds locally at the intersection, but that streamline routing significantly underestimates mixing when fractures are assumed to be parallel plates.

[58] As fractures are opened, flow and solute transport approach parallel plate approximations. As fractures are closed, flow channelization becomes increasingly important and mixing ratios increase. However, once flow paths other than the largest aperture channels are shut down, the pattern of flow around and through the intersection becomes fixed and increasing fracture closure may not increase mixing ratios.

[59] How apertures correlate across intersections has a large influence on mixing ratios, because the local distribution of flow around and through fracture intersections is set by high flow rate channels, which are in turn controlled by the apertures in the vicinity of the intersection. However, mixing is also significantly controlled by fracture apertures away from the intersection, since it is the interconnectivity of larger apertures that sets the flow channel locations and fluid fluxes.

[60] As with all flow and transport problems, the specific regimes of physical behavior observed here depend on the fluid flow rates, diffusion timescales, and the physical pore dimensions. Therefore to upscale or extrapolate these results outside of the laboratory, we would need to consider the relevant dimensionless parameters such as the Reynolds number and the Peclet number.

[61] **Acknowledgments.** This work was supported by the U.S. Department of Energy, Office of Basic Energy Sciences, Geosciences Research Program under contract DE-FG02-98ER14906. We thank Michael Nicholl and Steve Cox for comments that significantly improved the manuscript.

References

Berkowitz, B., and H. Scher (1998), Theory of anomalous chemical transport in random fracture networks, *Phys. Rev. E*, *57*, 5858–5869.

Berkowitz, B., C. Naumann, and L. Smith (1994), Mass transfer at fracture intersections: An evaluation of mixing models, *Water Resour. Res.*, *30*, 1765–1773.

Bourke, P. J. (1987), Channeling of flow through fractures in rock, in *Proc. of GEOVAL-87*, Swed. Nucl. Power Inspectorate, Stockholm.

Brown, S. (1987), Fluid flow through rock joints: The effect of surface roughness, *J. Geophys. Res.*, *92*, 1337–1347.

Brown, S. (1989), Transport of fluid and electrical current through a single fracture, *J. Geophys. Res.*, *94*, 9429–9438.

Brown, S. R. (1995), Simple mathematical model of a rough fracture, *J. Geophys. Res.*, *100*, 5941–5952.

Brown, S. R., H. W. Stockman, and S. J. Reeves (1995), Applicability of the Reynolds equation for modeling fluid flow between rough surfaces, *Geophys. Res. Lett.*, *22*, 2537–2540.

Brown, S., A. Caprihan, and R. Hardy (1998), Experimental observation of fluid flow channels in a single fracture, *J. Geophys. Res.*, *103*, 5125–5132.

Bruderer, C., and Y. Bernabe (2001), Network modeling of dispersion: Transition from Taylor dispersion in homogeneous networks to mechanical dispersion in very heterogeneous ones, *Water Resour. Res.*, *37*, 897–908.

Detwiler, R. L., S. E. Pringle, and R. J. Glass (1999), Measurement of fracture aperture fields using transmitted light: An evaluation of measurement errors and their influence on simulations of flow and transport through a single fracture, *Water Resour. Res.*, *35*, 2605–2617.

Detwiler, R. L., H. Rajaram, and R. J. Glass (2000), Solute transport in variable-aperture fractures: An investigation of the relative importance of Taylor dispersion and macrodispersion, *Water Resour. Res.*, *36*, 1611–1625.

Hu, Y., G. Mau, W. Cheng, and J. Zhang (2005), Theoretical and experimental study on flow distribution at fracture intersections, *J. Hydraul. Res.*, *43*, 321–327.

Hull, L. C., and K. N. Koslow (1986), Streamline routing through fracture junctions, *Water Resour. Res.*, *22*, 1731–1734.

Hull, L. C., J. D. Miller, and T. M. Clemo (1987), Laboratory and simulation studies of solute transport in fracture networks, *Water Resour. Res.*, *23*, 1513–1515.

Johnson, J. P., and S. R. Brown (2001), Experimental mixing variability in intersecting natural fractures, *Geophys. Res. Lett.*, *28*, 4303–4306.

Kitanidis, P. K. (1994), The concept of the dilution index, *Water Resour. Res.*, *30*, 2011–2026.

Kosakowski, G., and B. Berkowitz (1999), Flow pattern variability in natural fracture intersections, *Geophys. Res. Lett.*, *26*, 1765–1768.

Li, C. (1995), Low Peclet number mixing behavior at fracture junctions, Ph.D. thesis, 172 pp., N. M. Inst. of Min. and Technol., Socorro.

Li, G. (2002), Tracer mixing at fracture intersections, *Environ. Geol.*, *42*, 137–144.

Lyman, W. J., W. F. Reehl, and D. H. Rosenblatt (Eds.) (1990), *Handbook of Chemical Property Estimation Methods*, Am. Chem. Soc., Washington, D. C.

Mourzenko, V. V., F. Yousefian, B. Kolbah, J.-F. Thovert, and P. M. Adler (2002), Solute transport at fracture intersections, *Water Resour. Res.*, *38*(01), 1000, doi:10.1029/2000WR000211.

Nicholl, M. J., and R. Detwiler (2001), Simulation of flow and transport in a single fracture: Macroscopic effects of underestimating local head loss, *Geophys. Res. Lett.*, *28*, 4355–4358.

Nicholl, M. J., H. Rajaram, R. J. Glass, and R. Detwiler (1999), Saturated flow in a single fracture: Evaluation of the Reynolds equation in measured aperture fields, *Water Resour. Res.*, *35*, 3361–3373.

Oron, A. P., and B. Berkowitz (1998), Flow in rock fractures: The local cubic law assumption reexamined, *Water Resour. Res.*, *34*, 2811–2825.

Park, Y.-J., and K.-K. Lee (1999), Analytical solutions for solute transfer characteristics at continuous fracture junctions, *Water Resour. Res.*, *35*, 1531–1537.

Park, Y.-J., K.-K. Lee, and B. Berkowitz (2001), Effects of junction transfer characteristics on transport in fracture networks, *Water Resour. Res.*, *37*, 909–923.

Park, Y., K. Lee, G. Kosakowski, and B. Berkowitz (2003), Transport behavior in three-dimensional fracture intersections, *Water Resour. Res.*, *39*(8), 1215, doi:10.1029/2002WR001801.

Philip, J. R. (1988), The fluid mechanics of fracture and other junctions, *Water Resour. Res.*, *24*, 239–246.

Pyrak-Nolte, L. J., L. R. Myer, N. G. W. Cook, and P. A. Witherspoon (1987), Hydraulic and mechanical properties of natural fractures in low permeability rock, in *Proceedings of the Sixth International Congress on Rock Mechanics*, edited by G. Herget and S. Vongpaisal, pp. 225–231, A. A. Balkema, Brookfield, Vt.

Robinson, J. W., and J. E. Gale (1990), A laboratory and numerical investigation of solute transport in discontinuous fracture systems, *Ground Water*, *28*, 25–36.

Stockman, H. W., C. Li, and J. L. Wilson (1997), A lattice-gas and lattice Boltzmann study of mixing at continuous fracture junctions: Importance of boundary conditions, *Geophys. Res. Lett.*, *24*, 1515–1518.

Stockman, H. W., J. Johnson, and S. R. Brown (2001), Mixing at fracture intersections: influence of channel geometry and the Reynolds and Peclet numbers, *Geophys. Res. Lett.*, *28*, 4299–4302.

Thompson, M., and S. R. Brown (1991), The effect of anisotropic surface roughness on flow and transport in fractures, *J. Geophys. Res.*, *96*, 21,923–21,932.

S. Brown and J. Johnson, New England Research, 331 Olcott Drive, Ste L1, White River Junction, VT 05001-9263, USA. (sbrown@ner.com)

H. Stockman, Geochemistry Department, 6118, Sandia National Laboratories, P.O. Box 5800, Albuquerque, NM 87185-0750, USA.